Electrical, magnetic, and thermal properties of the single-grain $Ag_{42}In_{42}Yb_{16}$ icosahedral quasicrystal: Experiment and modeling

M. Bobnar,[1] S. Vrtnik,[1] Z. Jagličić,[2] M. Wencka,[3] Can Cui,[4] An Pang Tsai,[5] and J. Dolinšek[1,6,*]

[1]*Jožef Stefan Institute & University of Ljubljana, Faculty of Mathematics and Physics, Jamova 39, SI-1000 Ljubljana, Slovenia*

[2]*Institute of Mathematics, Physics and Mechanics & University of Ljubljana, Faculty of Civil and Geodetic Engineering, Jamova 2, SI-1000 Ljubljana, Slovenia*

[3]*Institute of Molecular Physics, Polish Academy of Sciences, Smoluchowskiego 17, 60-179 Poznań, Poland*

[4]*Department of Physics, Zhejiang Sci-Tech University, Hangzhou 310018, China*

[5]*Institute of Multidisciplinary Research for Advanced Materials, Tohoku University, Sendai 980-8577, Japan*

[6]*EN–FIST Centre of Excellence, Dunajska 156, SI-1000 Ljubljana, Slovenia*

(Received 19 May 2011; revised manuscript received 8 September 2011; published 17 October 2011)

We have investigated the anisotropy of physical properties (the magnetic susceptibility, the electrical resistivity, the thermoelectric power, the Hall coefficient, and the thermal conductivity) of single-grain icosahedral *i*-$Ag_{42}In_{42}Yb_{16}$ quasicrystal along the two-, three-, and fivefold symmetry directions of the crystallographic structure. The specific heat, being a scalar quantity, was determined as well. The symmetry analysis predicts that the tensorial physical properties reduce to scalars for the ideal icosahedral symmetry. The experiments have shown that the anisotropy of the electronic transport coefficients of *i*-$Ag_{42}In_{42}Yb_{16}$ is either small enough to be considered within the range of the experimental uncertainty (the electrical resistivity and the thermal conductivity) or negligible (the Seebeck and the Hall coefficients). The anisotropy of the magnetization and magnetic susceptibility was also found small, originating from different Yb^{3+} magnetic fractions (of the order 10^{-3} of all Yb atoms) determined along the three symmetry directions. Our experimental results support the consideration that perfect icosahedral quasicrystals should be isotropic solids regarding their physical properties, unlike decagonal quasicrystals that are strongly anisotropic. Theoretical reproduction of the temperature-dependent electron transport coefficients of *i*-$Ag_{42}In_{42}Yb_{16}$ by a spectral conductivity model was another aim of this paper.

DOI: 10.1103/PhysRevB.84.134205 PACS number(s): 61.44.Br, 71.23.Ft

I. INTRODUCTION

The anisotropic crystallographic structures of quasicrystals (QCs) generally result in anisotropic magnetic, electrical, and thermal transport properties, when measured along different crystallographic directions. The anisotropy of tensorial physical properties (the magnetic susceptibility, the electrical resistivity, the thermoelectric power, the Hall coefficient, and the thermal conductivity) of decagonal (*d*) QCs[1–9] and the decagonal approximant phases[10–16] is by now well established, both experimentally and theoretically. Depending on the crystallographic direction, the same crystal can exhibit either positive or negative thermoelectric power and Hall coefficient, or these parameters can change sign with the temperature.[14,15] The electrical resistivity along one crystallographic direction can be metal-like with a positive temperature coefficient (PTC), while it is insulator-like with a negative temperature coefficient (NTC) along another direction.[10] Likewise, the application of the magnetic field along one crystallographic direction can yield negative diamagnetic susceptibility, while it is positive paramagnetic along another direction.[12] The crystallographic structures of the *d*-QCs and their approximants can be conveniently described as a periodic stacking of atomic planes with either quasiperiodic in-plane atomic order in the case of *d*-QCs or translationally periodic order in the case of the approximants, where the stacking direction corresponds to the periodic 10-fold direction in the *d*-QCs or the pseudo-10-fold direction in the approximants. Common to all the investigated *d*-QCs[1–9] (*d*-Al-Ni-Co, *d*-Al-Cu-Co, and *d*-Al-Si-Cu-Co) and the decagonal approximant phases [Y-phase Al-Ni-Co,[12,13] $Al_4(Cr,Fe)$,[10,11] $Al_{13}Co_4$,[14] $Al_{13}Fe_4$, and $Al_{13}(Fe,Ni)_4$,[15] and the Taylor phase $Al_3(Mn,Fe)$[16] is the fact that the stacking direction was found the most conducting one for both the electricity and the heat. The stacking direction is also special to the magnetic properties of these compounds, as the application of the magnetic field along the stacking direction always results in weaker magnetism than for the in-plane application. The origin of the anisotropic electron transport coefficients of the *d*-QCs and their approximants is the anisotropic Fermi surface,[13–15] the anisotropy of which originates from the specific stacked-layer crystal structure and the chemical decoration of the lattice. The Fermi surface is composed of many branches (eleven in the Y-phase Al-Ni-Co[13] and eight in the orthorhombic $Al_{13}Co_4$ approximant[14]), containing pockets of electrons and holes, which are at the origin of the sign reversal of the thermopower and the Hall coefficient along different crystallographic directions.

The anisotropy of the physical properties of icosahedral (*i*) QCs has been investigated to a lesser extent. A perfect icosahedron has the largest finite group of symmetries in three dimensions (60 rotational symmetry elements about twofold, threefold, and fivefold rotation axes, and a symmetry order of 120, including transformations that combine a reflection and a rotation). In real *i*-QCs, inherent structural disorder locally corrupts the ideal icosahedral symmetry so that it is a question whether the structural anisotropy is large enough to produce anisotropy of the physical properties. The above issues were investigated on an icosahedral *i*-Ag-In-Yb single-grain quasicrystal by determining the magnetic susceptibility, the electrical resistivity, the thermoelectric power, the Hall

coefficient, and the thermal conductivity along the two-, three-, and fivefold symmetry directions of the structure. Theoretical reproduction of the temperature-dependent electron transport coefficients is another aim of this work. Here, we note that some physical properties of the polygrain *i*-Ag-In-Yb quasicrystal (the electrical resistivity, the thermopower, and the thermal conductivity) were already reported before.[17]

II. STRUCTURAL CONSIDERATIONS AND SAMPLE PREPARATION

The *i*-$Cd_{5.7}Yb$ is the first ever thermally stable binary icosahedral quasicrystal.[18,19] The *i*-$Cd_{5.7}Yb$ phase can be obtained as high-quality single grains; the binary phase exhibits good x-ray contrast between the Cd and Yb atoms; and the periodic approximant phases [the 1/1 Cd_6Yb (Refs. 20 and 21) and the 2/1 $Cd_{5.8}Yb$ (Refs. 21 and 22) cubic approximants] with almost the same chemical composition and known structures exist. These favorable conditions resulted in the most detailed structure solution of an *i*-QC achieved up to date.[23] Both the *i*-$Cd_{5.7}Yb$ QC and the approximant structures can be described as packing of interpenetrating large rhombic triacontahedral (RTH) clusters built up of five successive atomic shells [the outer-most RTH shell composed of 92 Cd atoms, a 30-atom Cd icosidodecahedron, a smaller Yb icosahedron (12 atoms), an even smaller Cd dodecahedron (20 atoms), and an inner Cd tetrahedron (4 atoms)]. In addition to the RTH clusters that comprise 93.8% of all the atoms of the structure, two additional basic building units, an acute and an obtuse rhombohedron, fill the remaining space in between the RTH clusters.

The *i*-$Cd_{5.7}Yb$ material is, however, not convenient for most experimental studies due to easy oxidation in air as well as high vapor pressure and toxicity of Cd. Instead, the Ag-In-Yb system is considered a better candidate for studying bulk single-grain *i*-QC properties, as it is stable in air and does not contain elements of high vapor pressure and toxicity.[24–27] The Ag-In-Yb phase diagram comprises an *i*-QC phase at the composition $Ag_{42}In_{42}Yb_{16}$ that is isostructural with the *i*-$Cd_{5.7}Yb$. In the *i*-$Ag_{42}In_{42}Yb_{16}$ phase, the Ag and In substitute in equal proportion the Cd atoms of the *i*-$Cd_{5.7}Yb$ phase. Since Ag and In have an atomic number one less and one more than Cd, respectively, the two phases are also isoelectronic. Two approximant phases, closely related to the *i*-QC in both the chemical composition and the local atomic structure [the 1/1 $Ag_{40}In_{46}Yb_{14}$ (Ref. 28) and the 2/1 $Ag_{41}In_{44}Yb_{15}$ (Ref. 29)], exist as stable phases in the Ag-In-Yb phase diagram as well.

Our centimeter-size single grain of *i*-$Al_{42}In_{42}Yb_{16}$ was grown by the Bridgman method. The natural growth direction of the grain was close to a twofold direction. Details of the material preparation and structural characterization can be found elsewhere.[27] We have cut from the parent grain three bar-shaped samples of approximate dimensions $1.3 \times 1.3 \times 5\ mm^3$ with their long axes along the two-, three-, and fivefold crystallographic directions. The brittleness of the material has caused some irregularities in the rectangular prism geometry of the samples, leading to a 10% geometrical error in the electrical resistivity determination. The samples were cut from a plane perpendicular to the twofold axis (the twofold plane), so that the orientation of one twofold axis perpendicular to the long axis of each sample was known as well. The samples prepared in that way enabled us to determine the physical properties along the three symmetry directions (two-, three-, and fivefold) of the icosahedral structure.

III. SYMMETRY ANALYSIS OF THE PHYSICAL PROPERTIES

In an anisotropic crystal, physical properties like the magnetic susceptibility χ, the electrical conductivity σ, the thermoelectric power S, and the thermal conductivity κ are symmetric (and diagonalizable) second-rank tensors. For example, the electrical conductivity tensor σ_{ij} relates the current density $\vec{j}$ to the electric field $\vec{E}$ via the relation $j_i = \sum_j \sigma_{ij} E_j$, where i, $j = x, y, z$ denote crystalographic directions in a Cartesian coordinate system. The Hall coefficient $R_H^{ijk} = E_j/j_i B_k$ is a third-rank tensor, with i, j, k denoting crystalographic directions of the current j_i, the Hall electric field E_j and the magnetic field B_k. The tensorial ellipsoids exhibit the same symmetry axes as the crystallographic structure. The invariance of the tensors on the symmetry operations of a given point group determines the form of the tensors. Using the icosahedral point group symmetry, we determine the general form of a second-rank tensor of an *i*-QC.

The icosahedron is a regular polyhedron with 20 identical equilateral triangular faces, 30 edges, and 12 vertices. In a Cartesian coordinate system, the vertices of an icosahedron with edge length 2, centered at the origin, are located at positions $(0, \pm 1, \pm\tau)$, $(\pm 1, \pm\tau, 0)$, and $(\pm\tau, 0, \pm 1)$, where $\tau = (1 + \sqrt{5})/2$ is the golden ratio. The 12 fivefold (C_5) axes pass from the origin through the vertices, the 20 threefold (C_3) axes pass through the centers of the triangles, and the 15 twofold (C_2) axes bisect the edges. The vertices form five sets of three concentric, mutually orthogonal golden rectangles (one set is shown in Fig. 1). Each of these rectangles defines

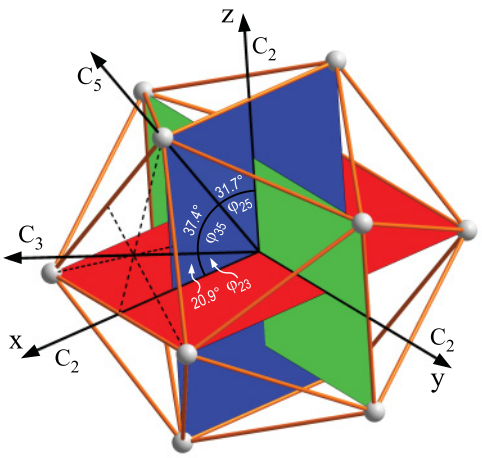

FIG. 1. (Color online) An icosahedron in a Cartesian coordinate system, with the x, y, z axes directed along three orthogonal C_2 axes. One set of three concentric, mutually orthogonal golden rectangles is shown as well. Each of these rectangles defines a twofold plane, where one C_2 axis is perpendicular to the plane, whereas two C_2 axes lie in plane. The C_5 and C_3 axes lie within the twofold planes at the angles $\phi_{23} = 20.9°$, $\phi_{25} = 31.7°$, and $\phi_{35} = 37.4°$.

a twofold plane, where one C_2 axis is perpendicular to the plane, whereas two C_2 axes lie in plane. Since the three C_2 axes are mutually perpendicular, they represent a convenient choice for the axes of a Cartesian x, y, z coordinate system. The C_5 and C_3 axes lie within the twofold planes at the angles $\phi_{23} = 20.9°$, $\phi_{25} = 31.7°$, and $\phi_{35} = 37.4°$ (Fig. 1). Due to the existence of C_2 axes in the x, y, and z directions, the off-diagonal elements of a symmetric second-rank tensor are zero by symmetry so that the tensor is diagonal in the above-defined coordinate system. Since the three orthogonal twofold planes are related by C_3 symmetry operations, the three diagonal elements of the tensor are equal, and the tensor becomes a scalar. A generalization of this result to the third-rank tensor (the Hall coefficient) is straightforward. Therefore, materials with ideal icosahedral symmetry should be isotropic regarding the physical properties. Any corruption of the perfect icosahedral symmetry in real materials may, however, introduce some anisotropy of the tensorial physical properties.

IV. EXPERIMENTAL RESULTS

Magnetic measurements were conducted by a Quantum Design MPMS XL-5 SQUID magnetometer equipped with a 50-kOe magnet, operating in the temperature range 1.9–400 K. The measurements of the electrical resistivity, the thermoelectric power, the Hall coefficient, the thermal conductivity, and the specific heat were conducted by a quantum design physical property measurement system (PPMS 9T) equipped with a 90-kOe magnet and operating in the temperature range 2–400 K. Electrical resistivity was measured by a standard four-terminal technique. The thermoelectric power and the thermal conductivity were measured simultaneously by monitoring both the temperature and voltage drop across the sample after a heat pulse is applied to its end by means of square waves. The Hall coefficient measurements were performed by the five-point method using standard ac technique in magnetic fields up to 10 kOe. The specific heat was measured by a thermal-relaxation calorimeter.

A. Magnetization and magnetic susceptibility

In the first set of measurements, the magnetic susceptibility $\chi = M/H$ was determined in the temperature range 1.9–300 K in magnetic fields $H = 1$ and 10 kOe applied along the two-, three-, and fivefold crystallographic directions (denoted as χ_2, χ_3, and χ_5). Since no field dependence of the susceptibility was found, we display and analyze in the following only the 1-kOe data [Fig. 2(a)]. The susceptibilities in all three directions exhibit a $1/T$ Curie-type paramagnetic temperature dependence, where χ_2 and χ_5 are almost equal in magnitude, and χ_3 is slightly larger. At $T > 70$ K, χ_2 and χ_5 become negative diamagnetic, whereas χ_3 remains slightly positive paramagnetic up to the highest investigated temperature of 300 K.

The temperature-dependent susceptibilities were analyzed by the Curie–Weiss law

$$\chi = \chi_0 + \frac{C}{T - \theta}, \tag{1a}$$

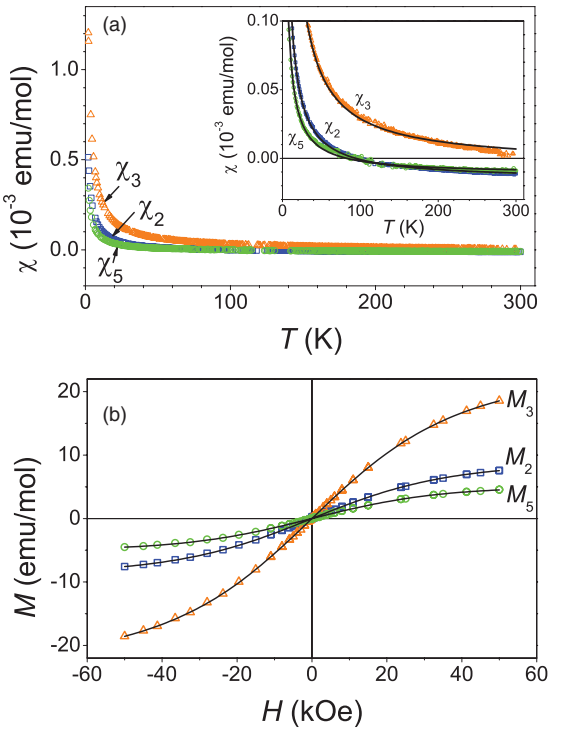

FIG. 2. (Color online) (a) Temperature-dependent magnetic susceptibility $\chi = M/H$ of i-$Ag_{42}In_{42}Yb_{16}$ in the field $H = 1$ kOe applied along the two-, three-, and fivefold symmetry directions. The inset shows the susceptibility on an expanded vertical scale. Solid curves are fits with Eq. (1a), and the fit parameters are given in Table I. (b) Magnetization vs the magnetic field, $M(H)$, determined at $T = 5$ K for the field applied along the two-, three-, and fivefold directions. Solid curves are fits with Eq. (1b) and the fit parameters are given in Table I.

where χ_0 is the temperature-independent part of the susceptibility, C the Curie–Weiss constant and θ the Curie–Weiss temperature. The constant C gives information on the magnitude of the Yb moments, whereas the type and strength of the coupling between the moments can be estimated from the magnitude and sign of θ. Theoretical fits with Eq. (1a) are shown as solid curves in Fig. 2(a), whereas the fit parameters are given in Table I. The temperature-independent part for the three directions is in the range $\chi_0 = (-15, -4.2) \times 10^{-6}$ emu/mol. The Larmor diamagnetic susceptibility of closed atomic shells for the $Ag_{42}In_{42}Yb_{16}$ composition was calculated from literature tables[30] to amount $\chi_{dia} = -21 \times 10^{-6}$ emu/mol, which is close to the value of χ_0, showing that χ_{dia} gives the dominant contribution to χ_0. The θ values were found very small and equal for all three directions, $\theta = -0.8$ K. The small θ should be considered as an additional fit parameter only, which slightly improves the fits. No other experimental results suggest any antiferromagnetic interaction between the magnetic moments.

The mean effective Bohr magneton number $\bar{p}_{eff}$ per Yb atom was calculated from the Curie−Weiss constant C using the formula[31] $\bar{p}_{eff} = 2.83\sqrt{C}$, where C is recalculated in unit per mol of Yb. We obtained the values $\bar{p}_{eff,2} = 0.27$, $\bar{p}_{eff,3} = 0.41$, and $\bar{p}_{eff,5} = 0.22$, which are strongly reduced with respect to the Bohr magneton number of a free Yb^{3+} ion ($p = 4.5$).

TABLE I. The temperature-independent term χ_0 of the susceptibility, the Curie–Weiss temperature θ, the Curie–Weiss constant C, the mean effective Bohr magneton number $\bar{p}_{\rm eff}$ per Yb atom, the Yb^{3+} magnetic fraction f calculated from $\bar{p}_{\rm eff}$, the saturated magnetization M_0 and the Yb^{3+} magnetic fraction f calculated from M_0. The parameter values were determined from the $\chi(T)$ and $M(H)$ fits shown in Fig. 2. All figures in units per mol are given per mol of $Ag_{0.42}In_{0.42}Yb_{0.16}$ molecules with the molar mass 121.21 g/mol.

Direction	χ_0 (emu/mol)	θ (K)	C (emu K/mol)	$\bar{p}_{\rm eff}$	f (from $\bar{p}_{\rm eff}$)	k (emu/mol)	M_0 (emu/mol)	f (from M_0)
Twofold	-15.6×10^{-6}	−0.8	14.8×10^{-4}	0.27	3.7×10^{-3}	-15.1×10^{-6}	11.0	3.1×10^{-3}
Threefold	-4.2×10^{-6}	−0.8	33.3×10^{-4}	0.41	8.3×10^{-3}	-3.6×10^{-6}	24.7	6.9×10^{-3}
Fivefold	-11.5×10^{-6}	−0.8	9.6×10^{-4}	0.22	2.4×10^{-3}	-21.1×10^{-6}	7.3	2.0×10^{-3}

Assuming that only a fraction $f = (\bar{p}_{\rm eff}/4.5)^2$ of all Yb atoms are in a magnetic Yb^{3+} state and carry the full magnetic moment, the rest of Yb being nonmagnetic Yb^{2+}, we obtained the magnetic Yb^{3+} fractions along the three crystallographic directions as $f_2 = 3.7 \times 10^{-3}$, $f_3 = 8.3 \times 10^{-3}$, and $f_5 = 2.4 \times 10^{-3}$. These values indicate that the magnetic Yb^{3+} moments are diluted in the sea of nonmagnetic Yb^{2+}. The almost zero Curie–Weiss temperatures θ indicate that the Yb^{3+} moments are uncoupled. Our *i*-$Ag_{42}In_{42}Yb_{16}$ QC samples can thus be classified as weak Curie paramagnets down to the lowest investigated temperature of 2 K, where a fraction of the order 10^{-3} of all Yb atoms are in a magnetic Yb^{3+} state, the rest being nonmagnetic Yb^{2+}. The magnetic Yb^{3+} fraction may either originate from a small number of Yb sites in the icosahedral lattice with different chemical bonding than the majority nonmagnetic Yb^{2+} sites, or the magnetic sites can be associated with defects in the lattice, i.e. Yb atoms in the vicinity of structural vacancies. The second option was investigated in detail in the icosahedral *i*-Al-Pd-Mn QCs, both experimentally and theoretically,[32] where it was shown that an increased concentration of defects results in an increased Mn magnetization.

In the second set of measurements, the magnetization vs the magnetic field curves $M(H)$ were determined at $T = 5$ K for the magnetic field applied along the two-, three-, and fivefold directions [Fig. 2(b)]. The magnetization curves show slight anisotropy, where M_2 and M_5 are almost equal in magnitude and M_3 is slightly larger, in agreement with the anisotropy order of the susceptibility. All three $M(H)$ curves show curvature typical of Curie-type paramagnets and were analyzed by the function

$$M = M_0 B_J(\mu H/k_B T) + kH. \quad (1b)$$

Here, M_0 is the saturated magnetization, B_J is the Brillouin function for the angular momentum J, and $\mu = Jg\mu_B$ is the magnetic moment, where μ_B is the Bohr magneton and g is the Landé factor [amounting to $g = 1.14$ for the Yb^{3+} ($J = 7/2$) state]. The parameter k represents terms in the susceptibility $\chi = M/H$ that are linear in the magnetic field (the Larmor core diamagnetic susceptibility and the susceptibility of the conduction electrons—the Pauli spin paramagnetic contribution and the Landau orbital diamagnetic contribution). The theoretical curves are shown as solid curves in Fig. 2(b), whereas the fit parameters are given in Table I. The values of the parameter k are, within the experimental precision, practically the same as the values of the temperature-independent susceptibility contribution χ_0 and about the same as $\chi_{\rm dia}$, showing that $\chi_{\rm dia}$ gives the dominant contribution to k. The saturated magnetization M_0 allows for an independent determination of the Yb^{3+} magnetic fraction f. Were all the Yb ions in a Yb^{3+} state, the total saturated magnetization would amount to $M_0^{\rm tot} = Jg\mu_B = 4.0\ \mu_B/Yb^{3+} = 3600$ emu/mol. The Yb^{3+} magnetic fraction is then obtained as $f = M_0/M_0^{\rm tot}$, yielding practically identical f values of the order 10^{-3} (last column in Table I) as when determined from the Curie–Weiss constant. The $M(H)$ analysis confirms the simple Curie-paramagnetic nature of noninteracting diluted Yb^{3+} moments in the investigated *i*-$Ag_{42}In_{42}Yb_{16}$ samples.

Regarding the experimentally observed weak anisotropy of the $\chi(T)$ and $M(H)$ curves along the two-, three-, and fivefold directions, its main origin is the different Yb^{3+} magnetic fractions f determined along the three symmetry directions.

B. Electrical resistivity

The electrical resistivity $\rho(T)$ data, measured between 300 and 2 K along the three symmetry directions are displayed in Fig. 3(a). All resistivities exhibit NTC with a tendency to level off to a constant value upon $T \to 0$. The weak anisotropy of the resistivity appears in the order $\rho_3 > \rho_2 > \rho_5$. At room temperature (RT), $\rho_3^{300K} = 201\ \mu\Omega$cm, and the resistivity increase to 2 K is by a factor $R_3 = (\rho_3^{2K} - \rho_3^{300K})/\rho_3^{300K} = 10\%$. For the other two directions, we have $\rho_2^{300K} = 188\ \mu\Omega$cm and $R_2 = 10\%$, whereas $\rho_5^{300K} = 181\ \mu\Omega$cm and $R_5 = 6\%$. The RT resistivity ratios amount to $\rho_3^{300K}/\rho_2^{300K} = 1.07$, $\rho_3^{300K}/\rho_5^{300K} = 1.11$, and $\rho_2^{300K}/\rho_5^{300K} = 1.04$ so that the RT anisotropy is up to 11%. The experimental error in the absolute values of the resistivity due to uncertainty in the determination of the samples' geometrical parameters (the length and the cross section) is estimated to 10%, so that the above differences between ρ_2, ρ_3, and ρ_5 are of the same order as the experimental error. In the case that the experimentally observed anisotropies would originate solely from the error in the geometrical parameters, ρ_2, ρ_3, and ρ_5 should differ just by constant scaling factors, having otherwise identical temperature dependence. The normalized resistivities $\rho(T)/\rho_{300K}$ along the three crystallographic directions are shown in Fig. 3(b). While the normalized ρ_2 and ρ_3 collapse perfectly onto a single curve in the entire temperature range, ρ_5 matches this curve from RT down to about 150 K, whereas at lower temperatures, it deviates slightly from a common curve, but the difference remains small. This deviation suggests that the geometrical error may not be the only source of the experimentally observed anisotropy, but another effect is present. Different concentration of defects along the investigated crystallographic directions seems a plausible

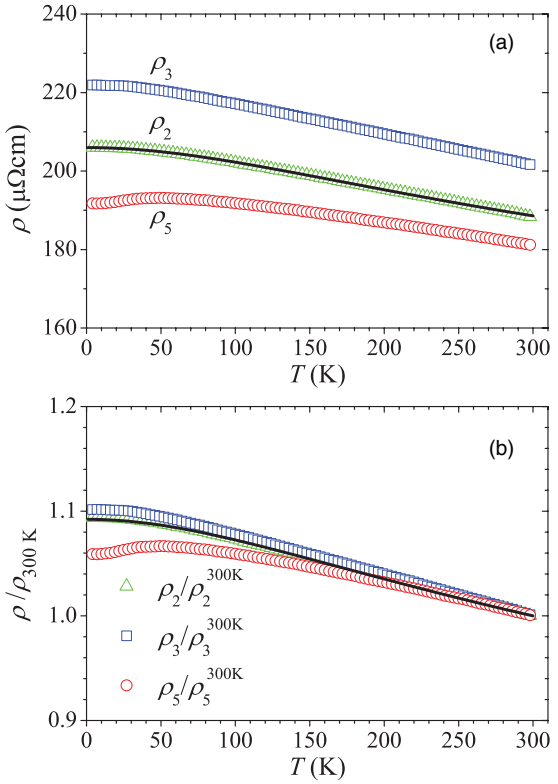

FIG. 3. (Color online) (a) Temperature-dependent electrical resistivity of i-$Ag_{42}In_{42}Yb_{16}$ along the two-, three-, and fivefold symmetry directions. (b) The normalized resistivities $\rho(T)/\rho_{300K}$ along the three symmetry directions. Solid curve is the fit with Eq. (3) using the spectral conductivity function $\sigma(\varepsilon)$ shown in Fig. 8.

explanation. According to the above results, no anisotropy of the resistivity beyond the experimental uncertainty can be claimed on the basis of our $\rho(T)$ experiments.

C. Thermoelectric power

The thermoelectric power data (the Seebeck coefficient S) of i-$Ag_{42}In_{42}Yb_{16}$, measured between 300 and 2 K along the two-, three-, and fivefold symmetry directions are displayed in Fig. 4. The thermopower is linearly positive for all three directions, and there is no anisotropy between the three directions, $S_2 = S_3 = S_5$. The RT value amounts to $S^{300K} = 14\ \mu$V/K, whereas upon $T \to 0$, S extrapolates approximately linearly to zero, a feature that is usually associated with metallic diffusion thermopower. The thermopower data show a tiny nonlinearity in the low-temperature range $T < 30$ K, a feature that is often associated with electron-phonon effects,[12] which typically reach their maximum value at a temperature that is some fraction of the Debye temperature θ_D. The linear positive thermopower is in agreement with the results obtained on the polygrain i-$Ag_{42}In_{42}Yb_{16}$ QC, where considerably stronger low-temperature nonlinearity was reported.[17]

D. Hall coefficient

The temperature-dependent Hall coefficient $R_H = E_y/j_x B_z$ was determined between 300 and 2 K. Three sets of experimental data were collected by directing the current j_x along the two-, three-, and fivefold symmetry directions, whereas the magnetic field B_z was always directed along the twofold direction perpendicular to the long axis of each sample. The three R_H data sets do not show any anisotropy beyond the experimental precision of $\pm 0.1 \times 10^{-10}$ m^{3}C^{-1} (Fig. 5). Here, R_H is small and practically temperature independent within the investigated temperature range; its average value amounts to $R_H \approx -0.2 \times 10^{-10}$ m^{3}C^{-1}.

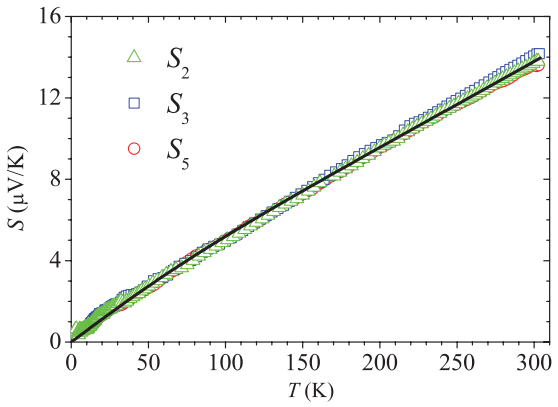

FIG. 4. (Color online) Temperature-dependent thermoelectric power (the Seebeck coefficient S) of i-$Ag_{42}In_{42}Yb_{16}$ along the two-, three-, and fivefold symmetry directions. Solid curve is the fit with Eq. (4) using the spectral conductivity function $\sigma(\varepsilon)$ shown in Fig. 8.

E. Thermal conductivity

The thermal conductivity κ along the two-, three-, and fivefold symmetry directions is displayed in Fig. 6. The RT values are small, in the range $\kappa^{300K} = 6$–7 W/mK. These low values are of the same order as those of i-Al-Pd-Mn QCs,[33,34] where they are considered to be a consequence of low electrical conductivity and the nonperiodicity of the lattice, strongly reducing both electronic and lattice contributions to heat transport. The anisotropy of κ along the three investigated crystalline directions is small and comparable to the experimental uncertainty. While no anisotropy was found between the twofold and fivefold directions, $\kappa_2 = \kappa_5$, small

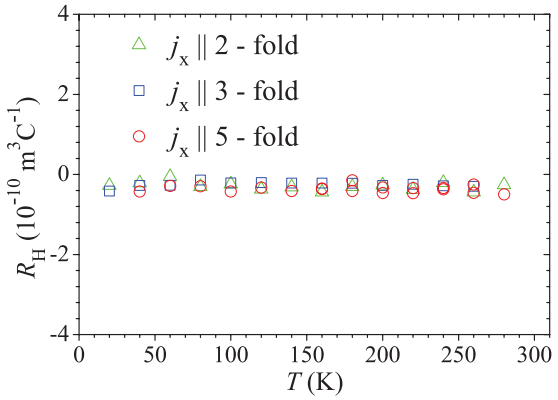

FIG. 5. (Color online) Temperature-dependent Hall coefficient $R_H = E_y/j_x B_z$ of i-$Ag_{42}In_{42}Yb_{16}$ for the current j_x along the two-, three-, and fivefold symmetry directions, whereas the magnetic field B_z was applied along the twofold direction perpendicular to the long axis of each sample.

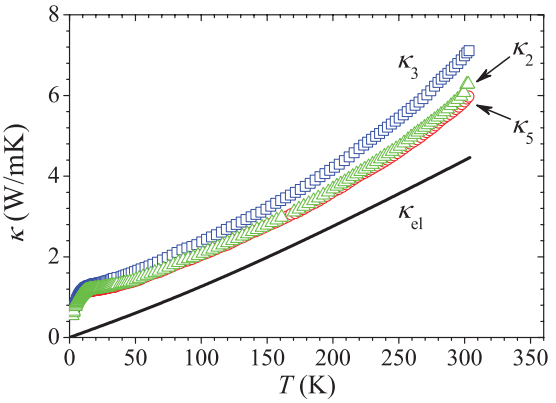

FIG. 6. (Color online) Thermal conductivity κ of i-$Ag_{42}In_{42}Yb_{16}$ along the two-, three-, and fivefold symmetry directions. Solid curve is the theoretical electronic contribution κ_{el}, calculated from Eq. (8) using the spectral conductivity function $\sigma(\varepsilon)$ shown in Fig. 8.

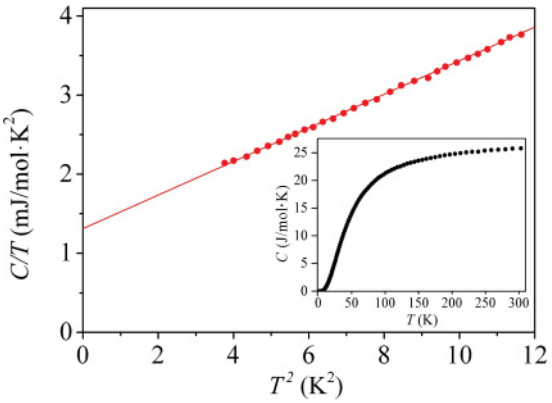

FIG. 7. (Color online) Low-temperature molar specific heat of i-$Al_{42}In_{42}Yb_{16}$ in a C/T vs T^2 plot. Solid line is the fit with Eq. (2). The specific heat in the entire investigated temperature range (2–300 K) is displayed in the inset.

anisotropy was found to the threefold direction, where at RT, $\kappa_3/\kappa_{2,5} = 1.17$.

F. Specific heat and the electronic density of states at ε_F

Though specific heat is a scalar quantity and hence does not give information on the anisotropic physical properties of i-Ag-In-Yb, the low-temperature specific heat $C(T)$ is a convenient quantity to estimate the value of the electronic density of states (DOS) at the Fermi energy ε_F and the Debye temperature θ_D. Neglecting the weak paramagnetism of the i-Ag-In-Yb, the total specific heat is a sum of the electronic and lattice specific heats. The electronic specific heat depends linearly on temperature, $C_{el}(T) = \gamma T$, where $\gamma = (\pi^2/3)k_B^2 g(\varepsilon_F)$ is the electronic specific heat coefficient and $g(\varepsilon_F)$ is the DOS at ε_F. At low temperatures below about 10 K, the lattice specific heat can usually be well approximated by the Debye model and is expressed as a function of temperature in the form $C_{latt}(T) = \alpha T^3$. The lattice specific heat coefficient α is related to the Debye temperature via the relation $\theta_D = (12\pi^4 R/5\alpha)^{1/3}$, where R is the gas constant. The total specific heat at low temperatures can then be written as

$$C(T) = \gamma T + \alpha T^3. \tag{2}$$

The specific heat measurements were performed in the temperature range between 2 and 300 K. The low-temperature molar specific heat of i-$Al_{42}In_{42}Yb_{16}$ is displayed in Fig. 7 in a C/T vs T^2 plot, whereas the specific heat is displayed in the inset for the whole investigated temperature range. The analysis yielded the values $\gamma = 1.27$ mJ/mol·K^2 and $\theta_D = 208$ K. It is instructive to compare the experimentally derived electronic specific heat coefficient γ to the corresponding free-electron value γ_F, calculated from[35] $\gamma_F = 0.136(A/d)^{2/3}(e/a)^{1/3}$ mJ/mol·K^2, where A is the molar mass in g, d the density in g/cm^3, and e/a the number of valence electrons per atom. For the i-$Al_{42}In_{42}Yb_{16}$, we take $A = 121.21$ g, $d \approx 8.88$ g/cm^3 (Ref. 23), and $e/a = 2$ (corresponding to the ionization states Ag^{1+}, In^{3+}, and Yb^{2+}), wherefrom we obtain $\gamma_F = 0.98$ mJ/mol·K^2. This yields the ratio $\gamma/\gamma_F = 1.30$, so that the experimental γ is 30% larger than the free-electron value. The deviations of γ in this range (10–40% higher than γ_F) are typically found even for free-electron-like metals like Na or Cu, where the increased γ is a consequence of the band structure and the many-body effects including electron-phonon and electron-electron interactions. Our result shows that the electronic specific heat coefficient γ of i-$Al_{42}In_{42}Yb_{16}$ is metallic-like and deviates from the free-electron value by a similar amount as it does in free-electron-like metals. The coefficient γ can be used to calculate the DOS value $g(\varepsilon_F)$, wherefrom we get $g(\varepsilon_F) = 0.586$ states/eV·atom, a value which is in agreement with the theoretical calculation for the 1/1 cubic approximant[28] of the i-Ag-In-Yb.

V. MODELING THE TEMPERATURE-DEPENDENT ELECTRON TRANSPORT COEFFICIENTS

The above-presented experimental results show that the anisotropy of the electronic transport coefficients of i-Ag-In-Yb is either small enough to be considered within the range of the experimental uncertainty (the electrical resistivity and the thermal conductivity) or negligible (the Seebeck and the Hall coefficients). In the following, we shall assume that all four transport coefficients are spatially isotropic (as also supported by the symmetry analysis) and perform the analysis of their temperature dependence using the spectral-conductivity model of Landauro and Solbrig.[36–38] Within this model, $\rho(T)$, $S(T)$, and $\kappa_{el}(T)$ are derived from a single energy-dependent spectral conductivity function $\sigma(\varepsilon)$, whereas $R_H(T)$ is derived from a spectral transverse conductivity in a magnetic field $\sigma_H(\varepsilon)$. Using the Kubo–Greenwood formalism, the temperature-dependent electrical conductivity is calculated from

$$\sigma(T) = \int d\varepsilon \sigma(\varepsilon) \left(-\frac{\partial f}{\partial \varepsilon}\right), \tag{3}$$

whereas the Seebeck coefficient is obtained from

$$S(T) = \frac{1}{eT\sigma(T)} \int d\varepsilon \sigma(\varepsilon)(\varepsilon - \mu) \left(-\frac{\partial f}{\partial \varepsilon}\right). \tag{4}$$

Here, e is the electric charge of the charge carriers (distinguishing between electrons and holes by its sign), $f = \{\exp[(\varepsilon - \mu)/k_B T] + 1\}^{-1}$ is the Fermi–Dirac function

and μ is the chemical potential, which is written in the low-temperature representation as[39]

$$\mu(T) \approx \varepsilon_F - (k_B T)^2 \frac{\pi^2}{6}\left[\frac{d\ln g(\varepsilon)}{d\varepsilon}\right]_{\varepsilon_F} = \varepsilon_F - \xi T^2. \quad (5)$$

The electronic DOS $g(\varepsilon)$ is related to the spectral conductivity via the Einstein relation $\sigma(\varepsilon) = (e^2/V)g(\varepsilon)D(\varepsilon)$ with $D(\varepsilon)$ being the electronic spectral diffusivity. The parameter ξ (or at least its starting value in the fit procedure) can be determined by recognizing that, in the case when the spectral variation of the electronic diffusivity can be neglected, one can replace $g(\varepsilon)$ by $\sigma(\varepsilon)$ in Eq. (5). Here, ξ can then be related to the thermopower using the Mott formula

$$S^{\mathrm{Mott}}(T) = \frac{\pi^2}{3}\frac{k_B^2}{e}\left[\frac{d\ln\sigma(\varepsilon)}{d\varepsilon}\right]_{\varepsilon_F} T, \quad (6)$$

yielding

$$\xi = \frac{e}{2}\frac{S^{\mathrm{Mott}}(T)}{T}. \quad (7)$$

The only material-dependent quantity in Eqs. (3) and (4) is $\sigma(\varepsilon)$ so that a proper model of the spectral conductivity should reproduce $\sigma(T)$ and $S(T)$ at the same time.

The electronic thermal conductivity κ_{el} is obtained as

$$\kappa_{el}(T) = \frac{L_{22}(T)}{e^2 T} - T\sigma(T)S^2(T), \quad (8)$$

where

$$L_{22}(T) = \int d\varepsilon \sigma(\varepsilon)(\varepsilon-\mu)^2\left(-\frac{\partial f}{\partial \varepsilon}\right), \quad (9)$$

and $\sigma(T)$ and $S(T)$ are given by Eqs. (3) and (4). Since $\kappa_{el}(T)$ is not explicitly obtained in the experiment (only the total thermal conductivity $\kappa(T)$ is measured), $\kappa_{el}(T)$ is then calculated theoretically by employing the spectral conductivity function $\sigma(\varepsilon)$ determined before from the simultaneous $\sigma(T)$ and $S(T)$ fits.

The magneto-transport is less clearly understood. As yet, even the question whether it can be explained as an on-the-energy-shell transport is not conclusively answered.[40] A widely used expression for the Hall coefficient is[41]

$$R_H(T) = \frac{1}{\sigma^2(T)}\int d\varepsilon \sigma_H(\varepsilon)\left(-\frac{\partial f}{\partial \varepsilon}\right). \quad (10)$$

However, the spectral transverse conductivity in the magnetic field, $\sigma_H(\varepsilon)$, is cumbersome to handle.[40] In a weak magnetic field B applied along the z direction, whereas the external and the Hall electric fields are in the x and the negative y directions, respectively, the spectral transverse conductivity is written as $\sigma_H(\varepsilon) = \sigma_{xy}(B,\varepsilon)/B$. Bush *et al.*[42] have suggested to relate $\sigma_H(\varepsilon)$ to the DOS derivative $-dg/d\varepsilon$. The assumption of an energy-independent electronic spectral diffusivity in the Einstein relation then allows transition to $-d\sigma(\varepsilon)/d\varepsilon$ just like in Eqs. (5) and (6), yielding

$$\sigma_H(\varepsilon) = Q(-d\sigma/d\varepsilon) \quad (11)$$

with a positive constant Q. The sign of the Hall coefficient is then determined by the sign of the (negative) derivative of the spectral conductivity $-d\sigma/d\varepsilon$. This has proved to be successful for the *i*-Al-Cu-Fe and *i*-Al-Cu-Ru(Si) QCs, where the DOS in the vicinity of the Fermi level forms a pseudogap.[43] Houari *et al.*[44] have reexamined this problem numerically. For substitutional disorder and weak scattering they confirmed that the sign of R_H is related to $-dg/d\varepsilon$. For topological disorder and strong scattering, however, the relation was not confirmed. Our purpose is to check whether the relation of Eq. (11) is fulfilled for the *i*-Ag-In-Yb QC.

Proper modeling of the spectral conductivity $\sigma(\varepsilon)$, pertinent to the *i*-Ag-In-Yb QC, is a crucial step to reproduce the temperature-dependent transport coefficients in the frame of the above theory. We first note that the experimentally observable part of $\sigma(\varepsilon)$ is determined by the thermal observation window $-\partial f/\partial\varepsilon$ that is a bell-shaped function centered at the chemical potential μ with a temperature-dependent full width at half maximum (FWHM) $\Delta_f = 3.5k_BT$. At $T = 300$ K, Δ_f amounts to 90 meV, whereas it becomes as small as 3 meV at 10 K. Upon $T \to 0$, $-\partial f/\partial\varepsilon$ becomes a delta function $\delta(\varepsilon - \varepsilon_F)$, and Eq. (3) yields the zero-temperature electrical resistivity $\rho_{T\to 0} = 1/\sigma(\varepsilon_F)$. The temperature-dependent chemical potential $\mu(T) = \varepsilon_F - \xi T^2$ is shifting the thermal observation window on the energy axis, so that different parts of $\sigma(\varepsilon)$ contribute to the integrals in Eqs. (3), (4), (9), and (10) at different temperatures. However, an estimate of ξ from Eq. (7), by using the thermopower data from Fig. 4 where $S^{300K} = 14\ \mu$V/K, yields $\xi = -0.023\ \mu$eV/K^2 so that the shift of the chemical potential from the Fermi energy at our highest measurement temperature of 300 K is very small, $\mu^{300K} - \varepsilon_F \approx 2$ meV. The shift of the chemical potential is thus almost negligible on the energy scale of the thermal observation window. In modeling the $\sigma(\varepsilon)$, only its portion in the interval of a few 100 meV around ε_F is experimentally relevant for the electronic transport coefficients.

Recent electronic structure calculations for the 1/1 Ag-In-Yb approximant of composition $Ag_{39}In_{47}Yb_{14}$ have revealed[28] that hybridization of the Yb 5*d* band with the Ag/In 5*p* band leads to a dip/pseudogap slightly above the Fermi level, with the Fermi level pinned to the negative-slope side of the pseudogap. An identical situation was found also for the Cd_6Yb approximant.[45,46] Since the experimentally observable part of $\sigma(\varepsilon)$ is determined by the thermal observation window, modelling the relevant part of $\sigma(\varepsilon)$ should employ a negative-sloping function with $(d\sigma/d\varepsilon)_{\varepsilon_F}\rangle 0$. Assuming that the electrons are the majority charge carriers ($e < 0$), the Mott formula of Eq. (6) then already qualitatively reproduces the linear and positive thermopower coefficient for such a functional form.

The modeling of $\sigma(\varepsilon)$ can be realized via many different mathematical functions. Here, we apply the functional form introduced by Landauro and Solbrig,[36–38] who modeled the spectral resistivity $\rho(\varepsilon) = 1/\sigma(\varepsilon)$ of *i*-Al-Cu-Fe by a superposition of two Lorentzians

$$\rho(\varepsilon) = A\left\{\left[\frac{1}{\pi}\frac{\gamma_1}{(\varepsilon-\delta_1)^2+\gamma_1^2}\right] + \alpha\left[\frac{1}{\pi}\frac{\gamma_2}{(\varepsilon-\delta_2)^2+\gamma_2^2}\right]\right\}, \quad (12)$$

where $1/\pi\gamma_i$ is the height of a Lorentzian, $2\gamma_i$ its FWHM, δ_i its position with respect to the Fermi energy (taken to be at the origin of the energy scale; $\varepsilon_F = 0$) and α is the relative

TABLE II. Parameters of the spectral resistivity $\rho(\varepsilon)$ of Eq. (13), obtained from the simultaneous fits of $\rho(T)$ and $S(T)$.

A $\mu\Omega$cm eV	δ_1 meV	γ_1 meV	α	δ_2 meV	γ_2 meV
11.74	5.9	58	53.3	682.9	546

weight of the Lorentzians. The set of parameters (A, α, δ_1, δ_2, γ_1, and γ_2) pertinent to $\rho(\varepsilon)$ was adjusted from simultaneous fits of the $\rho(T)$ and $S(T)$ data from Figs. 3 and 4 using Eqs. (3) and (4). The parameters are given in Table II, whereas the graph of $\sigma(\varepsilon)$ is shown in Fig. 8. In order to obtain converged results, we needed to integrate over an energy interval ± 10 $k_B T$ around ε_F, amounting to ± 0.26 eV at $T = 300$ K. On this scale, $\sigma(\varepsilon)$ is a negative-sloping function with a small dip at the Fermi level, where ε_F is pinned to the negative slope of the dip. The spectral conductivity at ε_F amounts to $\sigma(\varepsilon_F) = 4855\ \Omega^{-1}\text{cm}^{-1}$, yielding the zero-temperature resistivity $\rho_{T\to 0} = 1/\sigma(\varepsilon_F) = 206\ \mu\Omega$cm, in agreement with the experimental value averaged over the three investigated crystallographic directions. In Fig. 8, the thermal observation window $-\partial f/\partial\varepsilon$ at 300 and 40 K is shown as well. The parameter ξ value entering the temperature-dependent chemical potential was determined from the fits as $\xi = -0.028\ \mu\text{eV/K}^2$, which is almost identical to the starting value estimated from the Mott formula of Eq. (7).

Using the spectral conductivity from Fig. 8, the theoretical resistivity $\rho(T)/\rho_{300K}$ with $\rho_{300K} = 188\ \mu\Omega$cm and the thermopower $S(T)$ are shown as solid curves in Figs. 3(b) and 4, respectively. The fits reproduce quantitatively both the NTC resistivity and the PTC thermopower by assuming the electrons being the majority charge carriers. The positive thermopower is thus a consequence of the negative derivative $d\sigma/d\varepsilon < 0$ in the close vicinity of ε_F of an electronic (n type) conductor and not due to positive charge of p-type carriers (holes), as it might seem at first glance. The calculated electronic thermal conductivity $\kappa_{el}(T)$ using Eq. (8) is presented as solid curve in Fig. 6, suggesting that, at RT, the electrons transport about 70% of the heat, the rest being carried by the lattice. Since $\kappa_{el}(T)$ was not measured experimentally, we are not able to verify this prediction by comparing to the experiment. However, in view of the quite large electrical resistivity of i-Ag-In-Yb, the theoretical electronic contribution may be overestimated, and for that reason, we do not use it to extract the phononic part $\kappa_{ph} = \kappa - \kappa_{el}$ from the total thermal conductivity.

The analysis of the temperature-dependent Hall coefficient $R_H(T)$ using Eq. (10), by considering the spectral transverse conductivity $\sigma_H(\varepsilon)$ to be described by Eq. (11), did not yield the correct sign of the Hall coefficient. Equation (11) predicts that the sign of R_H equals the sign of the negative derivative of the spectral conductivity $-d\sigma/d\varepsilon$, which is positive for the spectral conductivity $\sigma(\varepsilon)$ of Fig. 8, whereas the experimental R_H of Fig. 5 is slightly negative. The relation of Eq. (11) is thus not confirmed for the i-Ag-In-Yb QC. Apart from failing to reproduce the sign of R_H, it is interesting to note that Eqs. (10) and (11) reproduce correctly the type of temperature dependence of $R_H(T)$ from Fig. 5 for the $\sigma(\varepsilon)$ of Fig. 8, where the almost temperature-independent $R_H(T)$ is a consequence of the fact that the derivative $-d\sigma/d\varepsilon$ is not changing much within the thermal observation window.

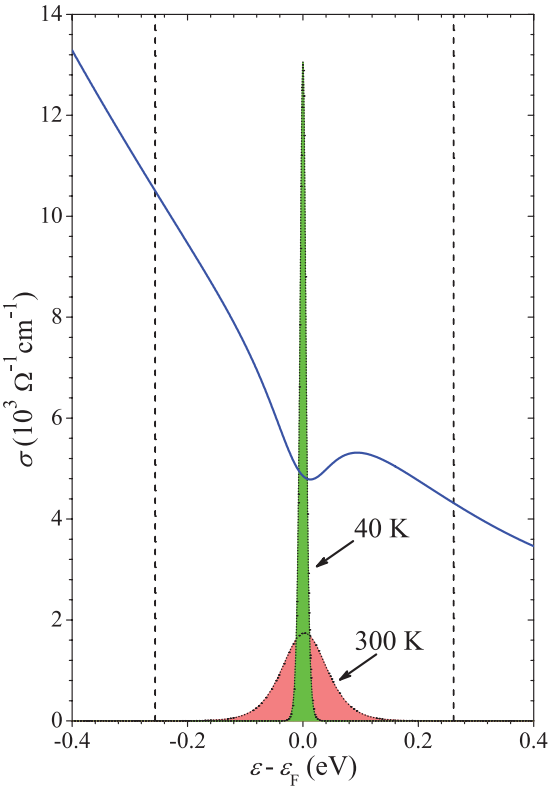

FIG. 8. (Color online) Spectral conductivity $\sigma(\varepsilon) = 1/\rho(\varepsilon)$ of Eq. (12) for the set of parameters from Table II, determined from the simultaneous fits of the electrical resistivity $\rho(T)$ and the thermopower $S(T)$. Dashed vertical lines denote the experimentally observable part of $\sigma(\varepsilon)$ at $T = 300$ K ($\pm 10\, k_B T$ around ε_F), determined by the thermal observation window $-\partial f/\partial\varepsilon$. The bell-shaped $-\partial f/\partial\varepsilon$ at 300 and 40 K (online colored pink and green, respectively) is shown by dotted curves as well (its vertical scale does not conform to the $\sigma(\varepsilon)$ scale).

VI. CONCLUSIONS

In order to investigate the anisotropy of physical properties of i-QCs, we determined the tensorial magnetic and transport properties (the magnetic susceptibility, the electrical resistivity, the thermoelectric power, the Hall coefficient, and the thermal conductivity) of a single-grain icosahedral i-$Ag_{42}In_{42}Yb_{16}$ quasicrystal along the two-, three-, and fivefold symmetry directions of the crystallographic structure. The specific heat, being a scalar quantity, was determined as well. The symmetry analysis has revealed that the tensors reduce to scalars for the icosahedral symmetry so that perfect i-QCs should be isotropic solids regarding their physical properties. Any corruption of the perfect icosahedral symmetry in real samples may, however, introduce some anisotropy of the tensorial physical properties. Our experimental results support these considerations, as the anisotropy of the electronic transport coefficients was found either small enough to be considered within the range of the experimental uncertainty (the electrical resistivity and the thermal conductivity) or negligible (the Seebeck and the Hall coefficients). The anisotropy of the magnetization and magnetic susceptibility was also found small, originating

from the different Yb^{3+} magnetic fractions (of the order 10^{-3} of all Yb atoms) determined along the three symmetry directions. The origin of the diluted Yb^{3+} moments in the sea of nonmagnetic Yb^{2+} may either be a small number of Yb sites in the icosahedral lattice with different chemical bonding than the majority nonmagnetic Yb^{2+} sites, or the magnetic sites can be associated with defects in the lattice, i.e. Yb atoms in the vicinity of structural vacancies. In the latter scenario, the weak anisotropy of magnetic properties could be associated with disorder-induced local corruption of the icosahedral symmetry, hence of extrinsic origin to the *i*-Ag-In-Yb phase. Due to the random character of the disorder, the slightly stronger disorder along the threefold direction could be accidental.

Theoretical reproduction of the temperature-dependent electron transport coefficients by a spectral conductivity model is another achievement of this work. Based on the literature-reported electronic structure calculations for the 1/1 Ag-In-Yb and the Cd_6Yb approximants, where the electronic DOS forms a dip/pseudogap slightly above the Fermi level with the Fermi level pinned to the negative-slope side of the pseudogap, we have modeled the spectral conductivity within the thermal observation window with a negative-sloping function. The model function has reproduced well the temperature-dependent electrical resistivity and the thermopower of *i*-$Ag_{42}In_{42}Yb_{16}$ in a simultaneous fit. The positive thermopower is a consequence of the negative derivative of the spectral conductivity in the close vicinity of ε_F of an electronic (*n* type) conductor. The theoretical consideration that the sign of the Hall coefficient should equal the sign of the negative derivative of the spectral conductivity was not confirmed.

ACKNOWLEDGMENTS

We thank Peter Gille for cutting the *i*-Ag-In-Yb samples along the crystallographic symmetry directions. CC acknowledges the support of Zhejiang Provincial Natural Science Foundation of China (Grant No. Y4100310).

*jani.dolinsek@ijs.si

[1] T. Shibuya, T. Hashimoto, and S. Takeuchi, J. Phys. Soc. Jpn. **59**, 1917 (1990).
[2] S. Martin, A. F. Hebard, A. R. Kortan, and F. A. Thiel, Phys. Rev. Lett. **67**, 719 (1991).
[3] Y. P. Wang and D. L. Zhang, Phys. Rev. B **49**, 13204 (1994).
[4] S. Y. Lin, X. M. Wang, L. Lu, D. L. Zhang, L. X. He, and K. X. Kuo, Phys. Rev. B **41**, 9625 (1990).
[5] D. L. Zhang, L. Lu, X. M. Wang, S. Y. Lin, L. X. He, and K. H. Kuo, Phys. Rev. B **41**, 8557 (1990).
[6] Y. P. Wang, D. L. Zhang, and L. F. Chen, Phys. Rev. B **48**, 10542 (1993).
[7] D. L. Zhang, S. C. Cao, Y. P. Wang, L. Lu, X. M. Wang, X. L. Ma, and K. H. Kuo, Phys. Rev. Lett. **66**, 2778 (1991).
[8] K. Edagawa, M. A. Chernikov, A. D. Bianchi, E. Felder, U. Gubler, and H. R. Ott, Phys. Rev. Lett. **77**, 1071 (1996).
[9] D. N. Basov, T. Timusk, F. Barakat, J. Greedan, and B. Grushko, Phys. Rev. Lett. **72**, 1937 (1994).
[10] J. Dolinšek, P. Jeglič, M. Komelj, S. Vrtnik, A. Smontara, I. Smiljanić, A. Bilušić, J. Ivkov, D. Stanić, E. S. Zijlstra, B. Bauer, and P. Gille, Phys. Rev. B **76**, 174207 (2007).
[11] J. Dolinšek, S. Vrtnik, A. Smontara, M. Jagodič, Z. Jagličić, B. Bauer, and P. Gille, Philos. Mag. **88**, 2145 (2008).
[12] A. Smontara, I. Smiljanić, J. Ivkov, D. Stanić, O. S. Barišić, Z. Jagličić, P. Gille, M. Komelj, P. Jeglič, M. Bobnar, and J. Dolinšek, Phys. Rev. B **78**, 104204 (2008).
[13] M. Komelj, J. Ivkov, A. Smontara, P. Gille, P. Jeglič, and J. Dolinšek, Solid State Commun. **149**, 515 (2009).
[14] J. Dolinšek, M. Komelj, P. Jeglič, S. Vrtnik, D. Stanić, P. Popčević, J. Ivkov, A. Smontara, Z. Jagličić, P. Gille, and Yu. Grin, Phys. Rev. B **79**, 184201 (2009).
[15] P. Popčević, A. Smontara, J. Ivkov, M. Wencka, M. Komelj, P. Jeglič, S. Vrtnik, M. Bobnar, Z. Jagličić, B. Bauer, P. Gille, H. Borrmann, U. Burkhardt, Yu. Grin, and J. Dolinšek, Phys. Rev. B **81**, 184203 (2010).
[16] M. Heggen, M. Feuerbacher, J. Ivkov, P. Popčević, I. Batistić, A. Smontara, M. Jagodič, Z. Jagličić, J. Janovec, M. Wencka, and J. Dolinšek, Phys. Rev. B **81**, 184204 (2010).
[17] Y. K. Kuo, K. M. Sivakumar, H. H. Lai, C. N. Ku, S. T. Lin, and A. B. Kaiser, Phys. Rev. B **72**, 054202 (2005).
[18] A. P. Tsai, J. Q. Guo, E. Abe, H. Takakura, and T. J. Sato, Nature **408**, 537 (2000).
[19] J. Q. Guo, E. Abe, and A. P. Tsai, Phys. Rev. B **62**, 14605 (2000).
[20] A. Palenzona, J. Less-Common Met. **25**, 367 (1971).
[21] C. P. Gómez and S. Lidin, Angew. Chem. Int. Ed. Engl. **40**, 4037 (2001).
[22] C. P. Gómez and S. Lidin, Phys. Rev. B **68**, 024203 (2003).
[23] H. Takakura, C. P. Gómez, A. Yamamoto, M. de Boissieu, and A. P. Tsai, Nat. Mater. **6**, 58 (2007).
[24] J. Q. Guo and A. P. Tsai, Philos. Mag. Lett. **82**, 349 (2002).
[25] H. R. Sharma, M. Shimoda, S. Ohhashi, and A. P. Tsai, Philos. Mag. **87**, 2989 (2007).
[26] S. Ohhashi, J. Hasegawa, S. Takeuchi, and A. P. Tsai, Philos. Mag. **87**, 3089 (2007).
[27] Can Cui and A. P. Tsai, J. Cryst. Growth **312**, 131 (2010).
[28] H. R. Sharma, G. Simutis, V. R. Dhanak, P. J. Nugent, C. Cui, M. Shimoda, R. McGrath, A. P. Tsai, and Y. Ishii, Phys. Rev. B **81**, 104205 (2010).
[29] M. R. Li, S. Hovmöller, J. L. Sun, X. D. Zou, and K. H. Kuo, J. Alloys Compd. **465**, 132 (2008).
[30] P. W. Selwood, *Magnetochemistry* (Interscience Publishers, New York, 1956), p. 78.
[31] F. E. Mabbs and D. J. Machin, *Magnetism and Transition Metal Complexes* (Chapman and Hall, London, 1973), p. 7.
[32] Z. Jagličić, M. Jagodič, B. Grushko, E. S. Zijlstra, Th. Weber, W. Steurer, and J. Dolinšek, Intermetallics **18**, 623 (2010).
[33] A. Bilušić, Ž. Budrović, A. Smontara, J. Dolinšek, P. C. Canfield, and I. R. Fisher, J. Alloys. Compd. **342**, 413 (2002).
[34] J. Dolinšek, P. Jeglič, P. J. McGuiness, Z. Jagličić, A. Bilušić, Ž. Bihar, A. Smontara, C. V. Landauro, M. Feuerbacher, B. Grushko, and K. Urban, Phys. Rev. B **72**, 064208 (2005).
[35] U. Mizutani, *Introduction to the Electron Theory of Metals* (Cambridge University Press, Cambridge, 2001), p. 39–42.
[36] C. V. Landauro and H. Solbrig, Mater. Sci. Eng. A **294–296**, 600 (2000).

[37]H. Solbrig and C. V. Landauro, in *Quasicrystals, Structure and Physical Properties*, edited by H. R. Trebin (Wiley-VCH, Weinheim, 2003), p. 254.

[38]C. V. Landauro and H. Solbrig, Physica B **301**, 267 (2001); C. V. Landauro, *Influence of Spectral Fine Structure on the Electronic Transport of Icosahedral Quasicrystals*, PhD Thesis, TU Chemnitz, 2002; http//archive.tu-chemnitz.de/pub/2002/.

[39]N. W. Aschroft and N. D. Mermin, *Solid State Physics* (Saunders College Publishing, London, 1976), p. 46.

[40]G. J. Morgan and M. A. Howson, J. Phys. C: Solid State Phys. **18**, 4327 (1985).

[41]N. E. Cusack, *The Physics of Structurally Disordered Matter* (Adam Hilger, Bristol and Philadelphia, 1987), p. 127.

[42]G. Bush and J. J. Güntherodt, Solid State Phys. **29**, 335 (1974).

[43]F. S. Pierce, P. A. Bancel, B. D. Biggs, Q. Guo, and S. J. Poon, Phys. Rev. B **47**, 5670 (1993).

[44]A. Houari, M. Mebrouki, A. F. R. Dib, and F. Ould-Kaddour, Physica B **291**, 387 (2000).

[45]Y. Ishii and T. Fujiwara, Phys. Rev. Lett. **87**, 206408 (2001).

[46]Y. Ishii and T. Fujiwara, J. Alloys Compd. **342**, 343 (2002).